

pubs.acs.org/acsapm Article

Frontal Polymerization of Thin Layers on a Thermally Insulating **Substrate**

Yuan Gao, Luis E. Rodriguez Koett, Julie Hemmer, Tianyu Gai, Nil A. Parikh, Nancy R. Sottos,* and Philippe H. Geubelle*

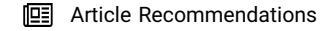


Cite This: ACS Appl. Polym. Mater. 2022, 4, 4919-4927

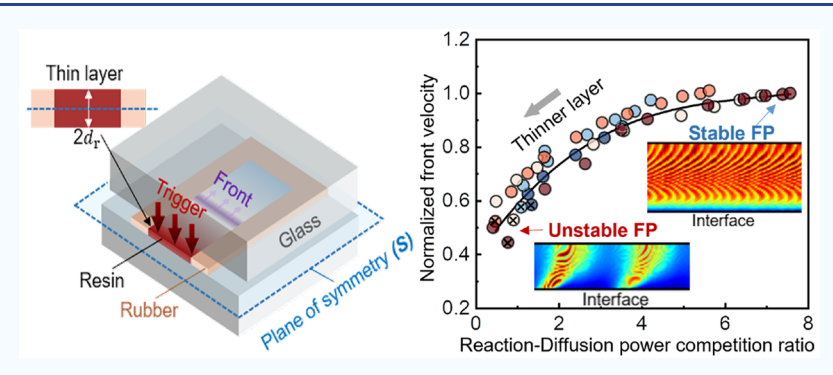


ACCESS I

Metrics & More



Supporting Information



ABSTRACT: Motivated by the use of frontal polymerization for the manufacturing of thin layers with thickness down to $\sim 100 \ \mu m_{\odot}$ we numerically and experimentally investigate the interplay between the exothermic polymerization and the heat losses to the substrate. The results show how the reaction-diffusion power balance affects the velocity and temperature of the polymerization front. The lower thickness limit of the thin layer depends on the cure kinetics of the resin and the thermal properties of the substrate and is described by a scaling law. Concurrently, thin-layer frontal polymerization experiments confirm the effects of front-substrate interaction on the front propagation and the limiting thickness of the polymerized layer. The present study offers a fundamental understanding of the resin-substrate interplay in thin-layer frontal polymerization and provides a quantitative description of the limiting thickness of the layer in the fabrication of functional thin polymeric parts and resin coatings.

KEYWORDS: frontal polymerization, thin layer, resin—substrate interface, thermochemical instability, reaction—diffusion power balance, multiphysical modeling

1. INTRODUCTION

A topic of resurgent interest in manufacturing high-performance polymers and composites, 1-6 frontal polymerization (FP), involves a self-propagating chemical reaction front usually initiated by a thermal stimulus, 7-13 which enables the rapid and energy-efficient curing of polymeric components.

The FP-based fabrication of thin layers with thickness down to $\sim 100 \ \mu m$ on a thermally insulating substrate has been achieved recently with reduced volatile organics emission¹⁴ and controllable initiation of curing, 15 which further broadens application of FP to the manufacturing of thin coat-^{6,17} Because the FP-based manufacturing of thin layers is characterized by a reduced availability of reaction heat, the thermal diffusion into the substrate plays a key role in this process.¹⁸ Therefore, leveraging the competition between the heat generated by the reaction and the thermal transport enables the tuning of key features that influence the efficiency and feasibility of FP, that is, the front shape, velocity, and temperature. 19,20 Moreover, thermochemical instabilities emerge at a critical reaction-thermal transport power balance, 21-28 potentially resulting in polymeric parts with complex geometries and heterogeneous properties.²⁹ A recent numerical study has reported that the resin layer thickness controls the front dynamics and determines its existence subject to convective heat loss.³⁰ Nevertheless, a quantitative relationship between front propagation, resin amount, and substrate effects is still lacking.

In the present work, we numerically and experimentally investigate the relationship between front propagation and interfacial thermal diffusion in the FP-based manufacturing of thin layers. Detailed calculations reveal that the power balance between reaction and diffusion governs the front velocity and temperature, leading to unstable front propagation when the

Received: March 22, 2022 Accepted: June 2, 2022 Published: June 10, 2022





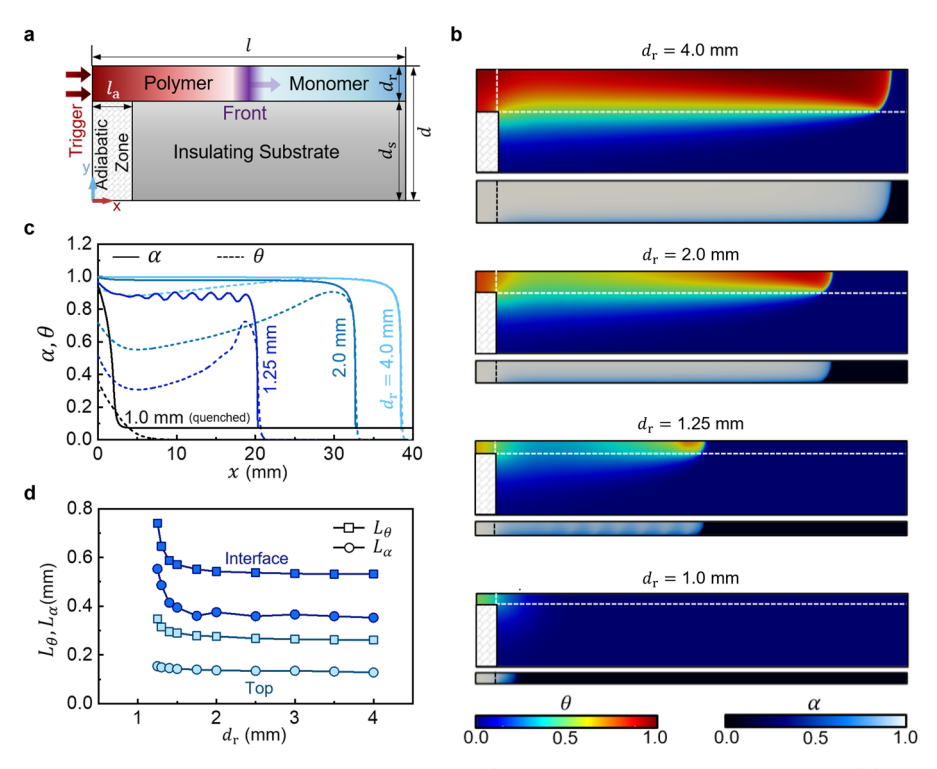


Figure 1. Simulation of thin-layer FP on a thermally insulating substrate. (a) Schematic of the simulated problem. (b) Distributions of normalized temperature θ and degree of cure α at time t=40 s after the thermal trigger for resin thickness values $d_r=4.0$, 2.0, 1.25, and 1.0 mm. (c) Spatial profiles of θ and α along the top boundary (y=d) for the solutions shown in (b). (d) Thermal (L_{θ}) and chemical (L_{α}) front widths as functions of the resin thickness d_r computed along the top boundary (y=d) and the resin—substrate interface $(y=d_s)$.

reaction power density is comparable to the diffusion power density. This power balance also determines the lower limit of resin thickness that is achievable through FP. A scaling law of the thickness limit is established according to the activation energy and processing temperature. Thin-layer FP experiments with resin sandwiched between a glass substrate and a glass lid validate the predicted FP features and thickness limit. Solvent-free dicyclopentadiene (DCPD) resin³¹ with enhanced reactivity and reaction heat was adopted.

2. COMPUTATIONAL AND EXPERIMENTAL METHODS

2.1. Numerical Modeling. The DCPD/ENB system was selected in the present work due to its high energy density, reactivity, and outstanding mechanical toughness and chemical resistance of the polydicyclopentadiene (pDCPD). The ring-opening metathesis polymerization reaction is described in Figure S1. As schematically shown in Figure 1a, FP of a thin layer of DCPD resin on a thermally insulating polydimethylsiloxane (PDMS) substrate is analyzed in a two-dimensional (2-D) numerical domain with a length l = 42 mm and a width $d = d_s + d_r$, where $d_s = 6$ mm represents the substrate thickness and d_r is the resin thickness set between 1 and 4 mm. Simulations performed with various values of the substrate thickness (Figure S2) have shown that $d_s = 6$ mm yields solutions similar to those associated with thicker substrates. A 2 mm long $(l_a = 2 \text{ mm})$ adiabatic zone is introduced near the trigger location to ensure that the front has reached a steady-state propagation before interacting with the substrate.

FP in the thin DCPD layer (denoted hereafter by the subscript r) is modeled by the following reaction—diffusion partial differential equations (PDEs) in terms of temperature T (in K) and degree of cure α (nondimensional):

$$\kappa_{\rm r} \frac{\partial^2 T}{\partial x^2} + \kappa_{\rm r} \frac{\partial^2 T}{\partial y^2} + \rho_{\rm r} H_{\rm r} \frac{\partial \alpha}{\partial t} = \rho_{\rm r} C_{p,\rm r} \frac{\partial T}{\partial t}$$

$$\frac{\partial \alpha}{\partial t} = A_{\rm r} \exp\left(-\frac{E_{\rm r}}{RT}\right) (1 - \alpha)^n \alpha^m \frac{1}{1 + \exp[c_{\rm d}(\alpha - \alpha_{\rm d})]}$$
(1)

In eq 1, $\kappa_{\rm r}$ (in W/(m K)), $C_{p,{\rm r}}$ (in J/(kg K)), and $\rho_{\rm r}$ (in kg/m³) respectively denote the thermal conductivity, heat capacity, and density of the resin and are listed in the first row of Table 1, 19 while

Table 1. Thermal Properties of Resin Layer and Substrate $Materials^{32-34}$

materials	κ (W/(m K))	$\rho (kg/m^3)$	$\binom{C_p}{(J/(kg\ K))}$	$D = \kappa/(\rho C_p) $ (m^2/s)
DCPD (r)	0.15	980	1600	9.57×10^{-8}
PDMS (s)	0.15	970	1460	1.06×10^{-7}
glass (s)	0.17	2215	800	9.59×10^{-8}

 $H_{\rm r}$ (in J/kg) represents the heat released by the exothermic reaction per unit mass. The thermal properties were assumed as constant in all simulations. The second equation approximates the cure kinetics of DCPD with the generalized Prout–Tompkins model and a molecular diffusion term. 29 $A_{\rm r}$ (in/s), $E_{\rm r}$ (in J/mol), and R (= 8.314 J/(mol K)) denote the pre-exponential factor, activation energy, and ideal gas constant, respectively. The exponents n and m correspond to the reaction order while the parameters $c_{\rm d}$ and $\alpha_{\rm d}$ describe the particle diffusion control regime of the reaction at higher values of the degree of cure. These parameters are summarized in Table 2.

Table 2. Cure Kinetic Parameters of DCPD³²

$A(s^{-1})$	E (J/mol)	n	m	$lpha_{ m d}$	c_{d}	$H_{\rm r}$ (J/kg)
8.55×10^{15}	110750	1.72	0.77	0.41	14.48	350000

The thermal diffusion in the substrate (denoted hereafter by the subscript s) is described by

$$\kappa_{s} \left(\frac{\partial^{2} T}{\partial x^{2}} + \frac{\partial^{2} T}{\partial y^{2}} \right) = \rho_{s} C_{p,s} \frac{\partial T}{\partial t}$$
(2)

Two thermally insulating substrates made of PDMS and glass are considered in this study, and their thermal properties in the modeling are summarized in the second and third rows of Table 1.

To solve these governing PDEs, the following initial and boundary conditions are applied:

$$\begin{split} T(x,y,0) &= T_0, \ 0 \leq x \leq l, \ d_s \leq y \leq d \& l_a \leq x \leq l, \ 0 \leq y \leq d \\ \alpha(x,y,0) &= \alpha_0, \ 0 \leq x \leq l, \ d_s \leq y \leq d \\ T(0,y,t) &= T_{\rm trig}, \ d_s \leq y \leq d, \ 0 \leq t \leq t_{\rm trig} \\ \frac{\partial T}{\partial x}(0,y,t) &= 0, \ d_s \leq y \leq d, \ t > t_{\rm trig} \end{split}$$

where T_0 (20 °C), α_0 (0.07), $T_{\rm trig}$ (200 °C), and $t_{\rm trig}$ (2 s) denote the initial temperature, initial degree of cure, triggering temperature, and triggering time, respectively. Adiabatic boundary conditions are applied along all other boundaries. At the resin–substrate interface, the continuity of temperature and heat flux was assumed.

The Multiphysics Object-Oriented Simulation Environment (MOOSE),³⁵ an open source C++ finite element solver possessing robust mesh and time-step adaptivity, is adopted in this study to capture the sharp temperature and degree-of-cure gradients in the vicinity of the advancing polymerizing front.

In the absence of the heat losses to the substrate or surroundings, and assuming that all the reaction heat is consumed to propagate the front, the front temperature is given by

$$T_{f,adia} = T_0 + \frac{H_r(1 - \alpha_0)}{C_{p,r}}$$
 (4)

according to which the temperature T can be normalized as

$$\theta = \frac{T - T_0}{T_{f,\text{adia}} - T_0} = \frac{(T - T_0)C_{p,\text{r}}}{H_{\text{r}}(1 - \alpha_0)}$$
(5)

In the results presented hereafter, the front position is denoted by the location where $\alpha=0.5$ since it is a unique value in the profile.³⁶ To determine the sharpness of the front, we adopt the following definitions for the thermal and chemical front widths:¹⁹

$$L_{\theta} = \frac{\theta_{\text{max}}}{\left|\frac{d\theta}{dx}\right|_{\text{max}}}, \quad L_{\alpha} = \frac{\alpha_{\text{max}}}{\left|\frac{d\alpha}{dx}\right|_{\text{max}}}$$
(6)

- **2.2. Experimental Methods.** 2.2.1. Materials. Dicyclopentadiene (DCPD), 5-ethylidene-2-norbornene (ENB), and secondgeneration Grubbs' catalyst (GC2) were all purchased from Sigma-Aldrich. Tributyl phosphite (TBP) was purchased from TCI America. All chemicals were used without further purification.
- 2.2.2. Resin Preparation. We added 5 wt % of ENB to DCPD to depress its melting point and allow it to remain liquid at room temperature. The mixture was left to degas overnight at room temperature and –100 kPa while stirring. Henceforth, all reference to DCPD refers to the resin system of 95:5 DCPD:ENB. For all experiments, 100 ppm of GC2 is weighed out into a scintillation vial. TBP is transferred via volumetric syringe into a desired amount of DCPD at 1 mol equiv with GC2. The DCPD/TBP mixture is aliquoted into the GC2 vial and then left to sonicate for 5 min for complete dissolution of the catalyst. All experiments were performed promptly after sonication.
- 2.2.3. Preparation of Thin-Layer Samples on Glass Substrates. Thin layers were manufactured by sandwiching a silicone rubber spacer between borosilicate glass plates (75 mm \times 75 mm \times 6 mm) both purchased from McMaster-Carr. The rubber spacer had a

rectangular cavity cut out to set the sample size to $25~\text{mm} \times 75~\text{mm}$, and its thickness was varied between 0.5 and 3 mm. Aluminum foil tape (Grainger Industrial Supply) was added to the rubber spacers for thicknesses of 0.8 and 0.9 mm. The final sample thickness was measured at three locations along the front propagation direction by using a digital micrometer. Liquid resin was transferred into the cavity by using a syringe to minimize bubble formation, thereby aiding in front tracking and front velocity measurements. FP was triggered with a resistance wire immersed in the cavity (4.4 V and 7.8 A for 3 s). Experiments at all studied thicknesses were performed three times to allow for standard deviation calculations.

2.2.4. Measurements of Front Velocity. Front propagation was captured by using a Canon EOS 7D digital camera, and front velocities were computed from the slope of the best-fit trendline obtained by postprocessing the video using the Tracker (ver. 5.1.5, open source) software. Each test with a target resin thickness was repeated at least three times.

2.2.5. Controls of Initial Temperature. The setup containing liquid resin was placed in a custom-built environmental chamber equipped with an AC-162 Peltier module, TC-720 temperature controller, and PS-24-25 power supply from TE Technology, Inc. For samples below room temperature, a thermocouple was then placed in the resin within the cavity to monitor the temperature prior to initiation, and the resin was placed in an MCB(H)-1.2 test chamber from Cincinnati Sub-Zero. Once the desired temperature (T_0) was reached and maintained for 5 min, the thermocouple was removed and the reaction was triggered.

2.2.6. Determination of Thickness Limit. For each initial temperature (T_0) , the rubber spacer thickness was incrementally increased until the front propagated along the entire cavity. The lower thickness limit $d_{\rm r,min}$ was defined as the minimum layer thickness needed to sustain a front. An average $d_{\rm r,min}$ was then computed from the maximum layer thickness at which the front quenched and the minimum thickness for which the front was observed to propagate.

3. RESULTS AND DISCUSSION

3.1. Thin-Layer Frontal Polymerization on a Thermally Insulating Substrate. Numerical solutions of the governing PDEs (1) and (2) for DCPD thin layers with $d_{\rm r}=4.0, 2.0, 1.25$, and 1.0 mm on a PDMS substrate are presented in Figure 1b. The fields of both normalized temperature θ (jet color scheme) and degree of cure α (blue color scheme) were obtained at t=40 s after the thermal trigger. At $d_{\rm r}=4$ mm, interfacial thermal transport across the resin—substrate interface dissipates part of the reaction heat, locally reducing the front temperature and leading to a curved front shape. After the passage of the front, the degree of cure close to the interface is lower than the interior part of the layer due to the interfacial thermal diffusion.

With reduced $d_{\rm r}=2$ mm, the available heat of reaction in the system decreases, but similar distributions of θ and α and a curved front shape are again observed. Compared to $d_{\rm r}=4$ mm, the front velocity is reduced and the temperature behind the front is lower. These phenomena are also demonstrated by α and θ profiles computed along the top boundary (y=d) in Figure 1c.

For $d_{\rm r}=1.25$ mm, the available reaction heat is further reduced, leading to lower values for the front velocity and temperature. Because of the increased cooling taking place behind the advancing front, the near-front thermal rise appears to be detached from the triggering zone. The degree-of-cure distribution is heterogeneous, suggesting the presence of thermochemical instabilities, as apparent in the oscillatory solution with a wavelength of about 1 mm obtained along y=d in Figure 1c. The front temperature drops due to the thermal

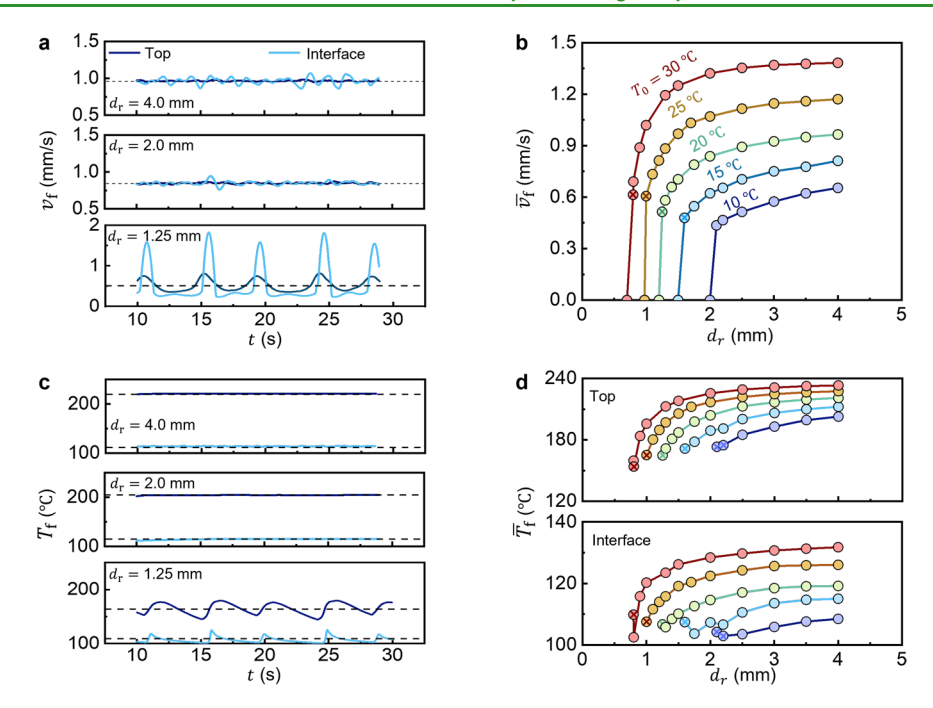


Figure 2. Evolution of the instantaneous front velocity $v_{\rm f}$ (a) and front temperature $T_{\rm f}$ (c) along the top boundary of the numerical domain (y=d) and the resin—substrate interface $(y=d_{\rm s})$ with resin thickness values $d_{\rm r}=4.0$, 2.0, and 1.25 mm, with the dashed lines denoting the average. Dependence of the average front velocity $\overline{v_{\rm f}}$ (b) and temperature $\overline{T_{\rm f}}$ (d) on the resin thickness $d_{\rm r}$ and the initial temperature T_0 . The circles containing the "X" symbol denote instances of thermochemical instability. The cases for which $\overline{v_{\rm f}}=0$ denote quenching of the front.

diffusion and the spatial heterogeneity in α thus remains after the FP (Figure S3).

When $d_{\rm r}=1.0$ mm, the front is quenched after leaving the adiabatic region, suggesting that the available heat of reaction is insufficient to drive the front propagation against the heat loss across the resin—substrate interface. Correspondingly, the 1-D profiles of α and θ along the top boundary rapidly drop to the corresponding initial values $\alpha_0=0.07$ and 0, respectively.

Figure 1d illustrates the dependence of the thermal L_{θ} and chemical L_{α} front widths on the resin thickness $d_{\rm r}$ at the interface $(y=d_{\rm s})$ and the top boundary of the numerical domain (y=d). At both locations, the thermal front precedes the degree-of-cure front to thermally trigger the chemical reaction (Figure S4), leading to $L_{\theta} > L_{\alpha}$ at each value of $d_{\rm r}$. The sharpness of both thermal and chemical fronts reduces with decreasing $d_{\rm r}$ due to the increasing role of thermal diffusivity. Moreover, both L_{θ} and L_{α} are higher along the resin—substrate interface $(y=d_{\rm s})$ than that along the top boundary (y=d) because of more significant thermal diffusion effects introduced by the substrate.

To quantify the effect of the layer thickness on the front speed, we present in Figure 2a the evolution of the instantaneous front velocity $v_{\rm f}$ computed along the top boundary and along the resin—substrate interface with $d_{\rm r}=4.0,\,2.0,\,{\rm and}\,1.25$ mm. In all cases, $v_{\rm f}$ is obtained from a linear regression (with a time window of 0.2 s) of the front location versus time solutions (Figure S5). During stable front propagation at $d_{\rm r}=4.0$ and 2.0 mm, $v_{\rm f}$ remains almost constant along the top boundary and only fluctuates slightly around its average (dashed lines) because of the interfacial thermal conduction. The average velocities at different $v_{\rm f}$ locations are the same. Significant periodic oscillations in $v_{\rm f}$ however, occur at $v_{\rm f}=1.25$ mm, for which the front propagation is unstable (Figure 1b,c). Furthermore, the results

shown in Figure 2a indicate that the average front velocity decreases as the layer thickness decreases.

The dependence of the average front velocity $\overline{v_{\rm f}}$ on the layer thickness $d_{\rm r}$ and initial temperatures T_0 is illustrated in Figure 2b, showing the aforementioned decreasing trend with respect to $d_{\rm r}$ and the quenching limit at which the $\overline{v_{\rm f}}$ drops to 0. In addition, a higher T_0 systematically leads to a higher value of $\overline{v_{\rm f}}$ because of the more active polymer chemistry according to eq 1 and to a reduced value of the lower thickness limit. Moreover, instabilities (marked by the "x" symbol) are observed at layer thickness values just above the quenched critical ones.

Figure 2c presents the evolution of the instantaneous front temperature $T_{\rm f}$ defined as the maximum temperature behind the front ($\alpha=0.5$). Similar to the evolution of $v_{\rm f}$ in Figure 2a, the periodic oscillations in $T_{\rm f}$ around its average (dashed lines) are clearly visible in the unstable FP case ($d_{\rm r}=1.25$ mm). Moreover, the average front temperature is higher along the top boundary than along the interface, as observed earlier in Figure 1b.

Just like $\overline{v_{\rm f}}$, the average front temperature $\overline{T_{\rm f}}$ increases with both $d_{\rm r}$ and T_0 (Figure 2d). However, at the interface, the higher $\overline{T_{\rm f}}$ of unstable fronts have a nonmonotonic dependence on $d_{\rm r}$ due to the thermal spikes. The effect of the layer thickness on front velocity and temperature is similar when FP is subjected to convective heat loss.

3.2. Reaction—Diffusion Power Balance. To understand the contrasting reaction-thermal-transport mechanisms during stable and unstable thin-layer FP with various d_r , we extract in Figure 3 the spatial variations in reaction rates $\frac{\partial \alpha}{\partial t}$ and interfacial thermal heat flux q_y over a subregion of length 10 mm. The maximum values, $\max\left(\frac{\partial \alpha}{\partial t}\right)$ and $\max(q_y)$, are directly related to the moment at which the front passes to a given

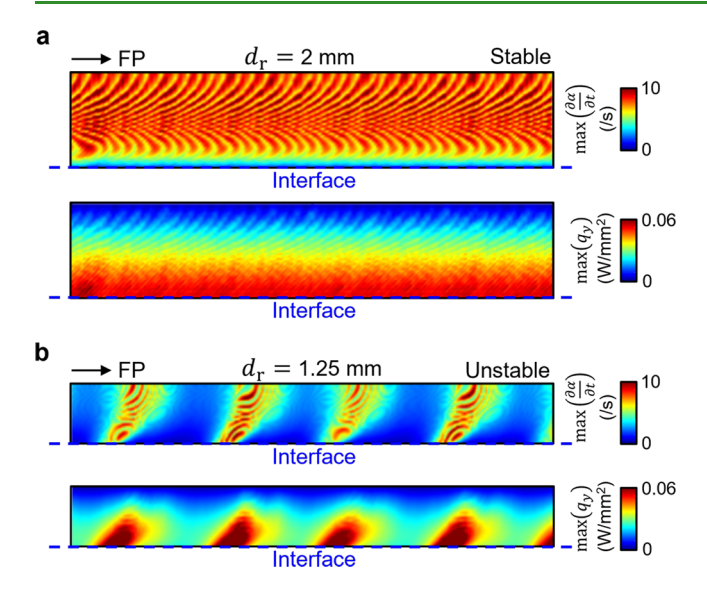


Figure 3. Spatial distributions of maximum reaction rate, $\max\left(\frac{\partial a}{\partial t}\right)$, and maximum heat flux in the *y*-direction, $\max(q_y)$, obtained for $T_0 = 20$ °C for layer thickness d_r of (a) 2 mm (stable front propagation) and (b) 1.25 mm (unstable front propagation).

location. During stable front propagation at $d_{\rm r}=2$ mm (Figure 3a), both ${\rm max}\Big(\frac{\partial \alpha}{\partial t}\Big)$ and ${\rm max}(q_y)$ exhibit slight fluctuations with a small, almost constant wavelength (\sim 0.1 mm) in the FP direction, which agrees with the small fluctuations in $\nu_{\rm f}$ and $T_{\rm f}$ alluded to in Figure 2a,c. In addition, the heat flux is highest near the resin–substrate interface, and ${\rm max}\Big(\frac{\partial \alpha}{\partial t}\Big)$ is therefore suppressed along the interface due to the thermal diffusion into

the substrate. Similar conclusions can be drawn with the $\max\left(\frac{\partial \alpha}{\partial t}\right)$ and $\max(q_y)$ contours with $d_r = 4.0$ mm (Figure S6).

When $d_{\rm r}$ is reduced to 1.25 mm, the effective reaction heat decreases, leading to thermochemical instabilities (Figure 3b). Significant periodic variations along the FP direction are observed in both $\max\left(\frac{\partial\alpha}{\partial t}\right)$ and $\max(q_y)$ with their peaks slightly mismatched. The peaks in $\max\left(\frac{\partial\alpha}{\partial t}\right)$ spatially lead those in $\max(q_y)$, which reflects a cyclic behavior in the power balance: the thermal diffusion rapidly dissipates the reaction heat, which is not sufficient to drive a stable front, and the front temperature drops (Figure 1c), suppressing both the chemical reaction and the thermal transport. Yet, the reduced front temperature and remaining reaction heat are sufficient to retrigger the polymerization reaction, leading to repeating cycles. The cyclic power balance in unstable FP generate heterogeneous thermal histories, which depend on $d_{\rm r}$ and T_0 (Figure S7).

To further quantify these observations, we adopt the concept of reaction, $P_{\rm R}$, and diffusion, $P_{\rm D}$, power densities²⁹ computed along the top boundary and along the resin—substrate interface as

$$P_{\rm R} = \rho_{\rm r} H_{\rm r} A \, \exp\left(-\frac{E}{R\overline{T}}\right), \quad P_{\rm D} = \kappa_{\rm r} \frac{\overline{T}}{L_{\theta}^2}$$
 (7)

where $\overline{T} = 0.5(T_0 + \overline{T_{\rm f}})$ is the average between the initial and average front temperatures. As shown in Figure 4a, $P_{\rm R}$ is much higher than $P_{\rm D}$ along the top boundary for $d_{\rm r} = 4$ mm, which indicates that the power generated by the reaction far exceeds the thermally dissipated power, leading to stable propagation at a almost constant front velocity and temperature (Figure 2a,c). As $d_{\rm r}$ decreases, $P_{\rm R}$ declines significantly due to its exponential

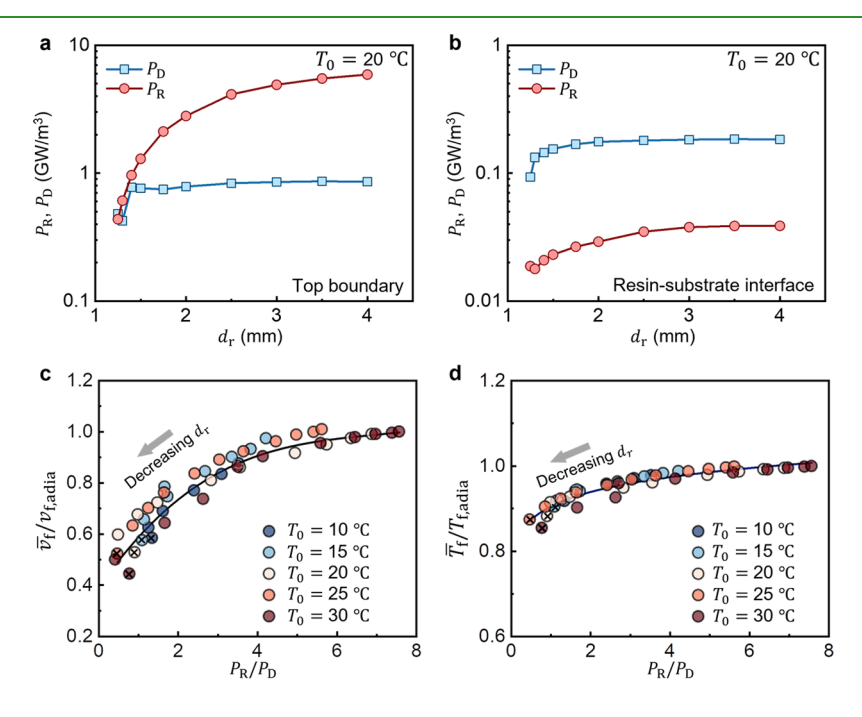


Figure 4. Power balance in thin-layer frontal polymerization on a substrate. Resin thickness $d_{\rm r}$ dependence of the reaction power density $P_{\rm R}$ and diffusion power density $P_{\rm D}$ computed (a) along the top edge of the layer and (b) along the layer—substrate interface. (c) Normalized front velocity $\overline{v_{\rm f}}/v_{\rm f,adia}$ and (d) front temperature $\overline{T_{\rm f}}/T_{\rm f,adia}$ versus $P_{\rm R}/P_{\rm D}$, where $v_{\rm f,adia}$ and $T_{\rm f,adia}$ are respectively the adiabatic front velocity and temperature (i.e., in the absence of heat diffusion into the substrate). The circles containing the "X" symbol denote instances of thermochemical instability.

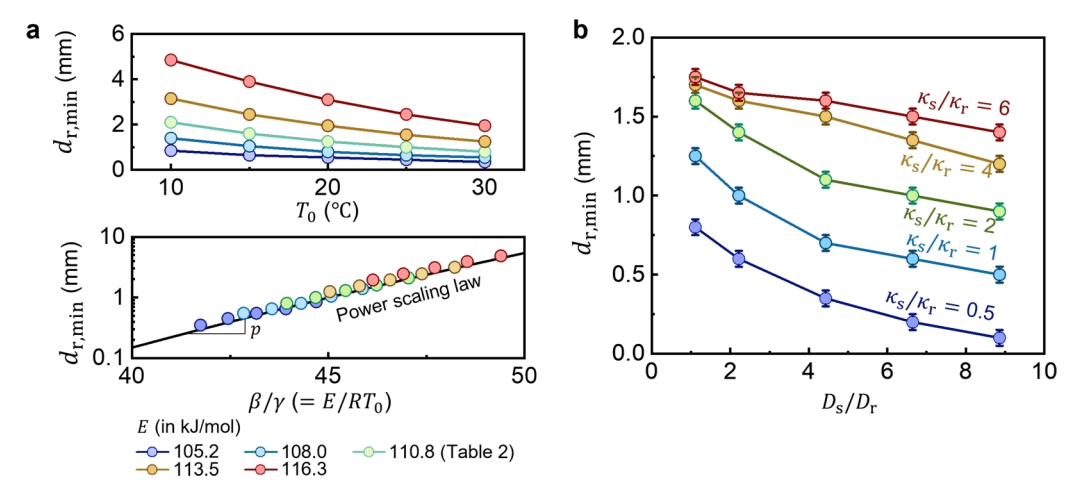


Figure 5. (a) Top: dependence of the lower thickness limit $d_{\rm r,min}$ on the initial temperature T_0 and activation energy E. Bottom: power scaling law of $d_{\rm r,min}$ with respect to the nondimensional parameter $\beta/\gamma = E/RT_0$. (b) Impact of the substrate-to-layer thermal diffusivity $D_{\rm s}/D_{\rm r}$ and thermal conductivity $\kappa_{\rm s}/\kappa_{\rm r}$ ratios on $d_{\rm r,min}$.

dependence on the decreasing $\overline{T_{\rm f}}$ (Figure 2c), while the diffusion power density $P_{\rm D}$ is slightly reduced because of the decreasing value of \overline{T} . When $P_{\rm R}$ and $P_{\rm D}$ are close in magnitude, unstable front propagation occurs (marked by "×" symbols). As $d_{\rm r}$ further decreases, the thermal diffusion dominates the power balance and rapidly diffuses the reaction heat. The remaining reaction heat is insufficient to sustain a front, and the FP is quenched. The quenched points are not shown in Figure 4b. A similar evolution of $P_{\rm R}$ and $P_{\rm D}$ is obtained for the cases $T_0=15$ and 25 °C (Figure S8).

Along the resin—substrate interface, the FP is more affected by the thermal diffusion into the substrate, which leads to a low front temperature (Figure 2d). Consequently, both $P_{\rm R}$ and $P_{\rm D}$ are substantially lower than those obtained along the top boundary (Figure 4b). Moreover, $P_{\rm D}$ is higher than $P_{\rm R}$ along the interface, which locally quenches the polymerization before α reaches 1 (Figure 1b and Figure S2).

Further analysis of the results obtained along the top boundary indicates that the normalized front velocity $\overline{v_f}/v_{f,\text{adia}}$ and temperature $\overline{T_f}/T_{f,\text{adia}}$ obtained with different initial temperature values T_0 show similar trends with respect to the power ratio P_R/P_D (Figures 4c and 4d, respectively). The reference front velocity $v_{f,\text{adia}}$ is obtained in the absence of the substrate (Figure S9). As the ratio P_R/P_D decreases, that is, as less reaction heat is generated against the thermal diffusion, both the front speed and temperature are reduced. Instabilities emerge at P_R/P_D values around 0.5, just above those leading to the quenching of the front.

3.3. Thickness Limit in Thin-Layer Frontal Polymerization. We next investigated the impact of the cure kinetics and the thermal properties of the substrate on the lower thickness limit $d_{r,\min}$ below which the FP is quenched. The PDE (1) for the resin are written in their nondimensional form:

$$\frac{\partial^2 \theta}{\partial \tilde{x}^2} + \frac{\partial^2 \theta}{\partial \tilde{y}^2} + \frac{\partial \alpha}{\partial \tau} = \frac{\partial \theta}{\partial \tau}$$

$$\frac{\partial \alpha}{\partial \tau} = \exp\left(-\frac{\beta}{\theta + \gamma}\right) g(\alpha)$$
(8)

where the variables of t, x, and y are respectively normalized as $\tau = At$, $\tilde{x} = x/\sqrt{\frac{\kappa_r}{\rho_r^A C_{p,r}}}$, $\tilde{y} = y/\sqrt{\frac{\kappa_r}{\rho_r^A C_{p,r}}}$. The nondimensional

form of the cure kinetics relation describing $\partial \alpha/\partial \tau$ introduces two dimensionless parameters, $\beta=\frac{EC_{p,r}}{RH_r}$ and $\gamma=\frac{T_0C_{p,r}}{H_r}$. Considering the same dependence on the degree of cure $g(\alpha)=\frac{(1-\alpha)^n\alpha^m}{1+\exp[c_d(\alpha-\alpha_d)]}$, the ratio $\gamma/\beta=RT_0/E$ appearing in the exponent captures the impact of the activation energy E and initial temperature T_0 .

To assess the impact of this ratio on the predicted lower thickness limit $d_{\rm r,min}$, we conducted a parametric study over a range of E and T_0 values presented in the upper subplot of Figure 5a, where $d_{\rm r,min}$ is determined with a precision of 0.5 mm. The adopted values of E and T_0 adopted in that parametric study lead to $v_{\rm f,adia}$ values ranging from \sim 0.1 to \sim 1 mm/s, which are typical for FP. 20 The green symbols correspond to the results obtained with the original value of E (110.8 kJ/mol) introduced in Table 2. As T_0 increases, the front temperature increases according to (4), and the polymerization front can be sustained with less heat of reaction, leading to a lower value for $d_{\rm r,min}$. Similarly, a lower E promotes the reaction rate according to the second relationship in (1), thereby reducing $d_{\rm r,min}$.

As illustrated in the lower subplot in Figure 5a, all these results can be captured through a power-law dependence of $d_{\rm r,min}$ on β/γ :

$$d_{\rm r,min} = d_{\rm r,0} (\beta/\gamma)^p \tag{9}$$

where the exponent p is found to be ~ 16.1 for the same reaction order, i.e., for the same function $g(\alpha)$.

To quantify the impact of the substrate properties on the lower thickness limit $d_{\rm r,min}$, we write the substrate PDE (2) in nondimensional form as

$$\frac{\partial^2 \theta}{\partial \tilde{x}^2} + \frac{\partial^2 \theta}{\partial \tilde{y}^2} = \frac{D_r}{D_s} \frac{\partial \theta}{\partial \tau} \tag{10}$$

In addition, the continuity of the heat flux across the resinsubstrate interface yields

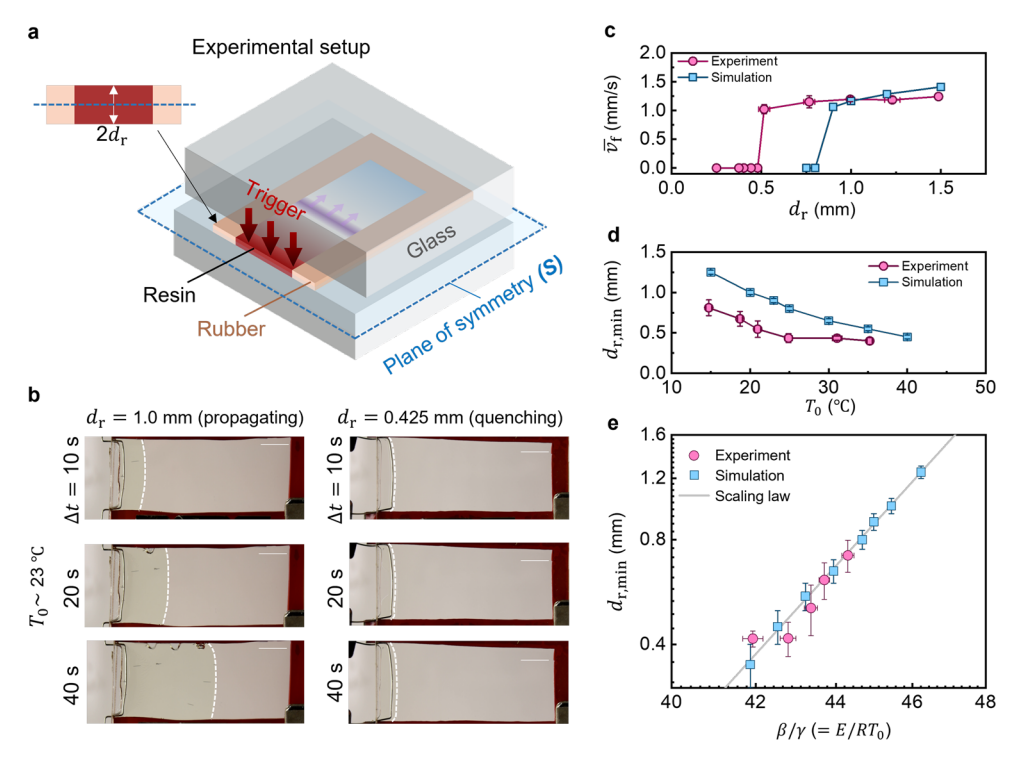


Figure 6. Experiments of FP in thin DCPD layers. (a) Schematic of the experimental setup and corresponding numerical model. (b) Optical images of the polymerization front for the resin thickness cases $d_{\rm r}=1.0$ and 0.425 mm, $T_0\sim 23$ °C. All scale bars represent 1 mm. (c) Experimental and numerical results of the dependence of the average front velocity $\overline{v_{\rm f}}$ on the resin thickness $d_{\rm r}$. (d) Lower thickness limit $d_{\rm r,min}$ as a function of the initial temperature T_0 in experiments and simulations. (e) Power scaling law of $d_{\rm r,min}$ in experiments and simulations based on the nondimensional parameter $\beta/\gamma=E/RT_0$ explored with a glass substrate.

$$\frac{\partial \theta}{\partial \tilde{y}_{r}} = \frac{\kappa_{s}}{\kappa_{r}} \frac{\partial \theta}{\partial \tilde{y}_{s}} \tag{11}$$

The nondimensionalization of the PDE and interface condition suggests that $d_{\rm r,min}$ is affected by two other nondimensional parameters that define the relative thermal properties of the substrate compared to those of the layer: the diffusivity ratio $D_{\rm s}/D_{\rm r}$ and the thermal conductivity ratio $\kappa_{\rm s}/\kappa_{\rm r}$. The results of a second parametric study of the effect of these two parameters for the case of a DCPD layer are presented in Figure 5b. In that study, the $D_{\rm s}$ and $\kappa_{\rm s}$ values were chosen around those of PDMS (Table 1) to represent a thermally insulating substrate. As expected, higher values of $\kappa_{\rm s}/\kappa_{\rm r}$ facilitate the thermal diffusion across the interface into the substrate and hinder the FP of the thin layer according to (11), thereby leading to higher values of $d_{\rm r,min}$ for a given $D_{\rm s}/D_{\rm r}$. A similar increase in $d_{\rm r,min}$ is obtained as the diffusivity ratio $D_{\rm s}/D_{\rm r}$ decreases for a given $\kappa_{\rm s}/\kappa_{\rm r}$.

3.4. Experiments. Figure 6a presents the schematic of the experimental setup described earlier. The resin is confined by glass substrates, thereby reducing convective heat loss. The absence of a free surface combined with the very small thickness of the resin greatly limits the potential impact of fluid convection in the frontal polymerization process. The resin thickness in the experimental setup is $2d_r$. As shown in Figure 6b, the polymerization front propagates across the entire cavity for $d_r = 1.0$ mm and quenches for $d_r = 0.425$ mm, which agrees qualitatively with the numerical results (Figures 1b and 2b). In some cases, air bubbles were observed along the spacer boundary but did not create porosity in the thin films.

More experiments were performed at room temperature (\sim 23 °C) for d_r ranging from 0.5 to 1.5 mm, and the average

front velocity $\overline{v_{\rm f}}$ results obtained via video postprocessing are presented in Figure 6c as pink symbols. As apparent in that figure, the front velocity slightly declines as $d_{\rm r}$ decreases, and the front quenches abruptly at $d_{\rm r}$ below $d_{\rm r,min}=0.5$ mm. In parallel, simulations with glass substrate and a reduced initial degree of cure $\alpha_0=0.01$ (small precure) were conducted (blue symbols), and the trend of $\overline{v_{\rm f}}$ with $d_{\rm r}$ is consistent with that in experiment. Owing to a higher heat of reaction $H_{\rm r}=381$ J/g for solvent-free DCPD, 31 the polymerization can be maintained with a smaller $d_{\rm r}=0.5$ mm in experiments.

Figure 6d summarizes the effect of initial temperature (T_0) on the lower thickness limit $(d_{\rm r,min})$ in experiments (pink symbols). The results highlight that a higher T_0 allows for sustained front propagation in thinner layers. Increasing the initial temperature promotes the polymerization reaction $(P_{\rm R})$, which can then be maintained with a smaller $d_{\rm r}$ and more pronounced thermal diffusion (i.e., lower $P_{\rm R}/P_{\rm D}$). A similar $d_{\rm r,min}-T_0$ relationship is observed with simulations (blue symbols). However, $d_{\rm r}$ in experiments are systematically lower than those in simulations due to the differences in cure kinetics.

Figure 6e indicates that the glass substrates lead to a different scaling law introduced in (9) with p=12.5, which generalize the experimental and numerical results with different cure kinetics. For experiments, the activation energy (E) was estimated as 106.1 kJ/mol with differential scanning calorimetry (DSC) measurements (Figure S10) and the Kissinger method.³⁷ The scaling law has been further confirmed numerically for a trimethylolpropane triacrylate (TMPTA) resin with nth-order cure kinetics (Figure S11).

4. CONCLUSION

With numerical simulations and experiments, we have shown that the frontal polymerization of a thin layer of resin on a thermally insulating substrate is governed by the reactiondiffusion power balance, which can be manipulated by changing the resin thickness, the environmental temperature, and the relative thermal diffusivity and conductivity of the substrate. A power scaling law has been proposed to predict the relationship between the lower thickness limit below which the front is quenched and the processing temperature. The existence of thermochemical instabilities has been shown numerically for values of the layer thickness and initial temperature close to the onset of front quenching. These results provide an energy-based fundamental understanding of the thin-layer polymerization on insulating substrates and lay the foundation for the manufacturing of functional thin layers and coatings.

ASSOCIATED CONTENT

5 Supporting Information

The Supporting Information is available free of charge at https://pubs.acs.org/doi/10.1021/acsapm.2c00497.

Ring-opening metathesis polymerization of the dicyclopentadiene resin; maximum temperature and degree-of-cure distributions; front trajectories during frontal polymerization; DSC measurements of the resin; power scaling law of the lower thickness limit explored with TMPTA resin (PDF)

AUTHOR INFORMATION

Corresponding Authors

Nancy R. Sottos — Beckman Institute of Advanced Science and Technology and Department of Materials Science and Engineering, University of Illinois, Urbana, Illinois 61801, United States; orcid.org/0000-0002-5818-520X; Phone: +1(217)333-1041; Email: n-sottos@illinois.edu

Philippe H. Geubelle — Beckman Institute of Advanced Science and Technology and Department of Aerospace Engineering, University of Illinois, Urbana, Illinois 61801, United States; orcid.org/0000-0002-4670-5474; Phone: + 1(217)244-7648; Email: geubelle@illinois.edu

Authors

Yuan Gao — Beckman Institute of Advanced Science and Technology and Department of Aerospace Engineering, University of Illinois, Urbana, Illinois 61801, United States; orcid.org/0000-0001-6030-9497

Luis E. Rodriguez Koett — Beckman Institute of Advanced Science and Technology and Department of Materials Science and Engineering, University of Illinois, Urbana, Illinois 61801, United States

Julie Hemmer — Beckman Institute of Advanced Science and Technology, University of Illinois, Urbana, Illinois 61801, United States

Tianyu Gai — Beckman Institute of Advanced Science and Technology and Department of Aerospace Engineering, University of Illinois, Urbana, Illinois 61801, United States

Nil A. Parikh – Beckman Institute of Advanced Science and Technology and Department of Aerospace Engineering, University of Illinois, Urbana, Illinois 61801, United States

Complete contact information is available at: https://pubs.acs.org/10.1021/acsapm.2c00497

Author Contributions

Y.G. and L.E.R.K. contributed equally to this work.

Notes

The authors declare no competing financial interest.

ACKNOWLEDGMENTS

This work was supported by the National Science Foundation for Grant 1933932 through the GOALI: Manufacturing USA: Energy Efficient Processing of Thermosetting Polymers and Composites. The authors also acknowledge the support from the U.S. Air Force Office of Scientific Research through Award FA9550-20-1-0194 as part of the Center of Excellence in Self-healing and Morphogenic Manufacturing.

REFERENCES

- (1) Brondsted, P.; Lilholt, H.; Lystrup, A. Composite Materials for Wind Power Turbine Blades. *Annu. Rev. Mater. Res.* **2005**, *35*, 505–538.
- (2) Friedrich, K.; Almajid, A. Manufacturing Aspects of Advanced Polymer Composites for Automotive Applications. *Appl. Compos. Mater.* **2013**, *20*, 107–128.
- (3) Chen, M.; Zhong, M.; Johnson, J. A. Light-Controlled Radical Polymerization: Mechanisms, Methods, and Applications. *Chem. Rev.* **2016**, *116*, 10167–10211.
- (4) Vernet, N.; Ruiz, E.; Advani, S.; Alms, J. B.; Aubert, M.; Barburski, M.; Barari, B.; Beraud, J. M.; Berg, D. C.; Correia, N.; Danzi, M.; Delaviere, T.; Dickert, M.; Di Fratta, C.; Endruweit, A.; Ermanni, P.; Francucci, G.; Garcia, J. A.; George, A.; Hahn, C.; Klunker, F.; Lomov, S. V.; Long, A.; Louis, B.; Maldonado, J.; Meier, R.; Michaud, V.; Perrin, H.; Pillai, K.; Rodriguez, E.; Trochu, F.; Verheyden, S.; Wietgrefe, M.; Xiong, W.; Zaremba, S.; Ziegmann, G. Experimental Determination of the Permeability of Engineering Textiles: Benchmark II. Composites, Part A 2014, 61, 172–184.
- (5) Armentano, I.; Bitinis, N.; Fortunati, E.; Mattioli, S.; Rescignano, N.; Verdejo, R.; López-Manchado, M. A.; Kenny, J. M. Multifunctional Nanostructured PLA Materials for Packaging and Tissue Engineering. *Prog. Polym. Sci.* **2013**, *38*, 1720–1747.
- (6) Peponi, L.; Puglia, D.; Torre, L.; Valentini, L.; Kenny, J. M. Processing of Nanostructured Polymers and Advanced Polymeric Based Nanocomposites. *Mater. Sci. Eng., R* **2014**, *85*, 1–46.
- (7) Davtyan, S.; Berlin, A.; Tonoyan, A. Advances and Problems of Frontal Polymerization Processes. *Rev. J. Chem.* **2011**, *1*, 56–92.
- (8) Pojman, J.; Curtis, G.; Ilyashenko, V. Frontal Polymerization in Solution. J. Am. Chem. Soc. 1996, 118, 3783–3784.
- (9) Mariani, A.; Bidali, S.; Fiori, S.; Sangermano, M.; Malucelli, G.; Bongiovanni, R.; Priola, A. UV-Ignited Frontal Polymerization of an Epoxy Resin. J. Polym. Sci., Part A: Polym. Chem. 2004, 42, 2066—2072.
- (10) Chen, S.; Tian, Y.; Chen, L.; Hu, T. Epoxy Resin/Polyurethane Hybrid Networks Synthesized by Frontal Polymerization. *Chem. Mater.* **2006**, *18*, 2159–2163.
- (11) Arutiunian, K. A.; Davtyan, S.; Rozenberg, B.; Enikolopyan, N. Curing of Epoxy Resins of Bis-phenol A by Amines Under Conditions of Reaction Front Propagation. *Dokl. Akad. Nauk. SSSR* **1975**, 223, 657–660.
- (12) Chekanov, Y.; Arrington, D.; Brust, G.; Pojman, J. A. Frontal Curing of Epoxy Resins: Comparison of Mechanical and Thermal Properties to Batch-Cured Materials. *J. Appl. Polym. Sci.* **1997**, *66*, 1209–1216.
- (13) Spade, C.; Volpert, V. On the Steady-State Approximation in Thermal Free Radical Frontal Polymerization. *Chem. Eng. Sci.* **2000**, *55*, *64*1–*654*.
- (14) Schieweck, A.; Bock, M.-C. Emissions from Low-VOC and Zero-VOC Paints—Valuable Alternatives to Conventional Formulations Also for Use in Sensitive Environments? *Build. Sci.* **2015**, *85*, 243–252.

- (15) Bansal, K.; Pojman, J. A.; Webster, D.; Quadir, M. Frontal Polymerization of a Thin Film on a Wood Substrate. *ACS Macro Lett.* **2020**, *9*, 169–173.
- (16) Holt, T.; Fazende, K.; Jee, E.; Wu, Q.; Pojman, J. A. Cure-on-Demand Wood Adhesive Based on the Frontal Polymerization of Acrylates. J. Appl. Polym. Sci. 2016, 133, 44064.
- (17) Knaack, P.; Klikovits, N.; Tran, A. D.; Bomze, D.; Liska, R. Radical Induced Cationic Frontal Polymerization in Thin Layers. *J. Polym. Sci., Part A: Polym. Chem.* **2019**, *57*, 1155–1159.
- (18) Goli, E.; Gai, T.; Geubelle, P. Impact of Boundary Heat Losses on Frontal Polymerization. J. Phys. Chem. B 2020, 124, 6404-6411.
- (19) Vyas, S.; Goli, E.; Zhang, X.; Geubelle, P. Manufacturing of Unidirectional Glass-Fiber-Reinforced Composites via Frontal Polymerization: A Numerical Study. *Compos. Sci. Technol.* **2019**, *184*, 107832.
- (20) Vyas, S.; Zhang, X.; Goli, E.; Geubelle, P. Frontal vs. Bulk Polymerization of Fiber-Reinforced Polymer-Matrix Composites. *Compos. Sci. Technol.* **2020**, *198*, 108303.
- (21) Goli, E.; Peterson, S. R.; Geubelle, P. H. Instabilities Driven by Frontal Polymerization in Thermosetting Polymers and Composites. *Composites, Part B* **2020**, *199*, 108306.
- (22) Masere, J.; Stewart, F.; Meehan, T.; Pojman, J. Period-Doubling Behavior in Frontal Polymerization of Multifunctional Acrylates. *Chaos* 1999, 9, 315–322.
- (23) Cardarelli, S.; Golovaty, D.; Gross, L.; Gyrya, V.; Zhu, J. A Numerical Study of One-Step Models of Polymerization: Frontal versus Bulk Mode. *Phys. D* **2005**, *206*, 145–165.
- (24) Comissiong, D.; Gross, L.; Volpert, V. Nonlinear Dynamics of Frontal Polymerization with Autoacceleration. *J. Eng. Math.* **2005**, *53*, 59–78.
- (25) Riolfo, L.; Carballido-Landeira, J.; Bounds, C.; Pojman, J.; Kalliadasis, S.; De Wit, A. Experimental Reaction-Driven Liquid Film Fingering Instability. *Chem. Phys. Lett.* **2012**, 534, 13–18.
- (26) Pojman, J.; Craven, R.; Khan, A.; West, W. Convective Instabilities in Traveling Fronts of Addition Polymerization. *J. Phys. Chem.* **1992**, *96*, 7466–7472.
- (27) Bowden, G.; Garbey, M.; Ilyashenko, V.; Pojman, J.; Solovyov, S.; Taik, A.; Volpert, V. Effect of Convection on a Propagating Front with a Solid Product: Comparison of Theory and Experiments. *J. Phys. Chem. B* **1997**, *101*, 678–686.
- (28) Gao, Y.; Dearborn, M. A.; Vyas, S.; Kumar, A.; Hemmer, J.; Wang, Z.; Wu, Q.; Alshangiti, O.; Moore, J. S.; Esser-Kahn, A. P.; Geubelle, P. H. Manipulating Frontal Polymerization and Instabilities with Phase-Changing Microparticles. *J. Phys. Chem. B* **2021**, 125, 7537–7545
- (29) Lloyd, E. M.; Feinberg, E. C.; Gao, Y.; Peterson, S. R.; Soman, B.; Hemmer, J.; Dean, L. M.; Wu, Q.; Geubelle, P. H.; Sottos, N. R.; Moore, J. S. Spontaneous Patterning during Frontal Polymerization. *ACS Cent. Sci.* **2021**, *7*, 603–612.
- (30) Tiani, R.; Pojman, J. A.; Rongy, L. Critical Role of Layer Thickness in Frontal Polymerization. *J. Phys. Chem. B* **2022**, 126, 3607–3618.
- (31) Ivanoff, D. G.; Sung, J.; Butikofer, S. M.; Moore, J. S.; Sottos, N. R. Cross-Linking Agents for Enhanced Performance of Thermosets Prepared via Frontal Ring-Opening Metathesis Polymerization. *Macromolecules* **2020**, *53*, 8360–8366.
- (32) Robertson, I.; Yourdkhani, M.; Centellas, P.; Aw, J.; Ivanoff, D.; Goli, E.; Lloyd, E.; Dean, L.; Sottos, N.; Geubelle, P.; Moore, J.; White, S. Rapid Energy-Efficient Manufacturing of Polymers and Composites via Frontal Polymerization. *Nature* **2018**, *557*, 223.
- (33) Mark, J. E. Polymer Data Handbook; Oxford University Press: 2009.
- (34) Borosilicate Glass Sheet; https://www.mcmaster.com/8476K32/
- (35) Gaston, D.; Newman, C.; Hansen, G.; Lebrun-Grandie, D. MOOSE: A Parallel Computational Framework for Coupled Systems of Nonlinear Equations. *Nucl. Eng. Des.* **2009**, 239, 1768–1778.
- (36) Gao, Y.; Dearborn, M. A.; Hemmer, J.; Wang, Z.; Esser-Kahn, A. P.; Geubelle, P. H. Controllable Frontal Polymerization and

Spontaneous Patterning Enabled by Phase-Changing Particles. Small 2021, 17, 2102217.

(37) Hardis, R.; Jessop, J. L.; Peters, F. E.; Kessler, M. R. Cure Kinetics Characterization and Monitoring of an Epoxy Resin Using DSC, Raman Spectroscopy, and DEA. *Composites, Part A* **2013**, *49*, 100–108.

□ Recommended by ACS

Dewetting Dynamics of Sheared Thin Polymer Films: An Experimental Study

Anna Dmochowska, Guillaume Miquelard-Garnier, et al.

MARCH 11, 2022 ACS MACRO LETTERS

READ 🗹

Drying Kinetics from Micrometer- to Nanometer-Scale Polymer Films: A Study on Solvent Diffusion, Polymer Relaxation, and Substrate Interaction Effects

Tobias Börnhorst, Wilhelm Schabel, et al.

MAY 05, 2021 LANGMUIR

READ 🗹

Atomistic Modeling of Dual-Cured Thermosets Based on Glycidyl Methacrylate and Hardeners with Various Architecture and Functionality

Baris Demir.

SEPTEMBER 15, 2021

ACS APPLIED POLYMER MATERIALS

READ 🗹

Effect of Polymer on the Contact Line Friction of a Capillary Bridge

Eunsang Lee and Florian Müller-Plathe

MARCH 17, 2022 MACROMOLECULES

READ 🗹

Get More Suggestions >